COBEM 2023 27TH INTERNATIONAL CONGRESS OF MECHANICAL ENGENEERING

ABCM Brazilian Society of Mechanical Sciences and Engineering
27th ABCM International Congress of Mechanical Engineering
December 04-08, 2023, Florianópolis-SC, Brazil

COB-2023-2429
DYNAMICAL ANALYSIS OF A HELICAL GEAR PAIR WITH BACKLASH UNDER VARIABLE LOAD TORQUE CONDITIONS

Laís Bitencourt Visnadi
Aline Souza de Paula
Departament of Mechanical Engineering, University of Brasília, Brasília-DF, Brazil
lais.visnadi@unb.br
alinedepaula@unb.br

Abstract. *Wind turbine gearboxes are subjected to fluctuating torque conditions, which may generate vibration problems. This paper analyzes the mesh displacement of a helical gear pair, inspired by the challenges posed in simulating the high-speed stage of the wind turbine gearbox. The detailed mesh model, considering static transmission error, time-varying mesh stiffness, and backlash, associated with a 12-degree-of-freedom gear pair model better represents this system. The model also takes into account a load torque factor to prevent over-speed conditions. Results show a comparison between the system's response in the absence of backlash and when backlash is introduced. When there is no backlash, both the driving and driven gears exhibit quasi-periodic behavior. When there is a backlash, single-sided impacts occur along the permanent response of the gear system, a severe vibration condition that may cause damage to the system.*

Keywords: *Wind turbine, Helical gear pair, Transmission error, Gear backlash, Gear dynamics.*

1. INTRODUCTION

The aim to reduce gas emissions that cause climate change has raised interest in clean energy production. In this context, research about wind turbines has been increased, regarding both efficiency and reliability. The gearbox is an essential component of the wind turbine since it increases the rotor speed to the required generator speed, and its failure is a significant concern in the design and operation of these systems (Ragheb and Ragheb, 2010).

In most cases, the gearbox consists of one or two planetary gear stages and one or two parallel shaft stages (Teng *et al.*, 2014). Geared systems present internal excitation generated by tooth contact. This contact is often modeled by time-varying stiffness due to gear tooth geometry and the number of pairs in contact at the same time (Yang and Lin, 1987). Additionally, models also take into account assembling and manufacturing variability as a static transmission error. Imperfect gear assembly is further considered by incorporating backlash into the model (Özgüven, 1991). Various authors, such as Wei *et al.* (2015) and Wang *et al.* (2014), have addressed these nonlinearities through torsional models. As high loads on the shafts may cause gear center displacements and the gear mesh helix angle couples all the directions of motion, a 12-degree of freedom model, as proposed by Kahraman (1994), may better represent this system dynamics.

Fluctuations in wind patterns result in varying torque levels on the rotor. To achieve maximum efficiency and to guarantee the generator operates within its safe limits, avoiding any over-speed conditions, speed control is essential (Apata and Oyedokun, 2020). Large torques and torque variations can cause contact loss on the gearbox, generating vibration problems (Zhao and Ji, 2015).

The present work proposes an analysis of the behavior of a gear pair, subjected to torque variations, simulating the high-speed parallel stage. In the context of wind turbines, this shaft is connected to the electric generator. The mesh model considers all the characteristics mentioned and a 12 DOF lumped parameter model for the gear pair, including gyroscopic effects is used. The model encompasses backlash phenomena and incorporates a load torque consideration to mitigate the risk of over-speed conditions.

2. METHODOLOGY

A lumped parameter model of a helical gear pair was considered to simulate the system. Figure 1 shows gear 1 and gear 2 translational coordinates (y_1, x_1, z_1, y_2, x_2, and z_2), gear mesh representation (the line composed by $2b$, $e(t)$ and $k_m(t)$), helix angle (β), position angle (Ψ), driving torque ($T_1(t)$) and load torque ($T_2(t)$).

Gears' supports may not be perfectly rigid, so both gears centers can translate and also rotate in all directions (i.e. there are six more degrees of freedom in this gear pair, which are θ_{y1}, θ_{x1}, θ_{z1}, θ_{y2}, θ_{xg2}, and θ_{z2}) and then gyroscopic effects may occur. The system's equations of motion, considering gravity forces, are obtained by Lagrange's Equation (Kubur *et al.*, 2004):

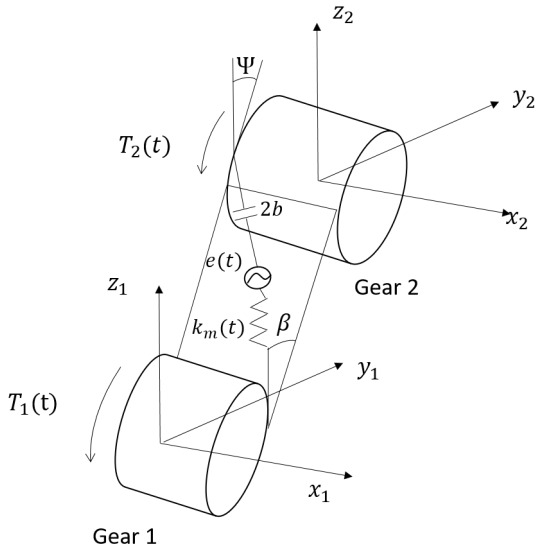

Figure 1. Helical gear pair scheme. Adapted from Kubur *et al.* (2004)

$$m_1\ddot{y}_1 + k_m\left(t\right)h\left[p\left(t\right)\right]\cos\left(\beta\right)\sin\left(\Psi\right) + C_{s_1}\dot{y}_1 + K_{s_1}y_1 = 0, \tag{1}$$
$$m_1\ddot{z}_1 + k_m\left(t\right)h\left[p\left(t\right)\right]\cos\left(\beta\right)\cos\left(\Psi\right) + C_{s_1}\dot{z}_1 + K_{s_1}z_1 = -m_1 g, \tag{2}$$
$$m_1\ddot{x}_1 + k_m\left(t\right)h\left[p\left(t\right)\right]\cos\left(\beta\right)\cos\left(\Psi\right) + C_{s_1}\dot{x}_1 + K_{s_1}x_1 = 0, \tag{3}$$
$$I_1\ddot{\theta}_{y1} + r_{b1}k_m\left(t\right)h\left[p\left(t\right)\right]\sin\left(\beta\right)\sin\left(\Psi\right) + \dot{\theta}_{x1}J_1\dot{\theta}_{z1} + C_{\theta s_1}\dot{\theta}_{y1} + K_{\theta s_1}\theta_{y1} = 0, \tag{4}$$
$$I_1\ddot{\theta}_{z1} + r_{b1}k_m\left(t\right)h\left[p\left(t\right)\right]\sin\left(\beta\right)cos(\Psi) - \dot{\theta}_{x1}J_1\dot{\theta}_{y1} + C_{\theta s_1}\dot{\theta}_{z1} + K_{\theta s_1}\theta_{z1} = 0, \tag{5}$$
$$J_1\ddot{\theta}_{x1} + r_{b1}k_m\left(t\right)h\left[p\left(t\right)\right] + \cos\left(\beta\right) = T_1(t), \tag{6}$$
$$m_2\ddot{y}_2 - k_m\left(t\right)h\left[p\left(t\right)\right]\cos\left(\beta\right)\sin\left(\Psi\right) + C_{s_2}\dot{y}_2 + K_{s_2}y_2 = 0, \tag{7}$$
$$m_2\ddot{z}_2 - k_m\left(t\right)h\left[p\left(t\right)\right]\cos\left(\beta\right)\cos\left(\Psi\right) + C_{s_2}\dot{z}_2 + K_{s_2}z_2 = -m_2 g, \tag{8}$$
$$m_2\ddot{x}_2 - k_m\left(t\right)h\left[p\left(t\right)\right]\cos\left(\beta\right)\cos\left(\Psi\right) + C_{s_2}\dot{x}_2 + K_{s2}x_2 = 0, \tag{9}$$
$$I_2\ddot{\theta}_{y2} + r_{b2}k_m\left(t\right)h\left[p\left(t\right)\right]\sin\left(\beta\right)\sin\left(\Psi\right) + \dot{\theta}_{x2}J_2\dot{\theta}_{z2} + C_{\theta s_2}\dot{\theta}_{y2} + K_{\theta s_2}\theta_{y2} = 0, \tag{10}$$
$$I_2\ddot{\theta}_{z2} + r_{b2}k_m\left(t\right)h\left[p\left(t\right)\right]\sin\left(\beta\right)cos(\Psi) - \dot{\theta}_{x2}J_g\dot{\theta}_{y2} + C_{\theta s_2}\dot{\theta}_{z2} + K_{\theta s_2}\theta_{z2} = 0, \tag{11}$$
$$J_2\ddot{\theta}_{x2} + r_{b2}k_m\left(t\right)h\left[p\left(t\right)\right]\cos\left(\beta\right) = T_2(t), \tag{12}$$

where m indicates mass, C_s indicates support damping, K_s indicates support stiffness, g is the acceleration of gravity, I indicates moment of inertia, J indicates polar moment of inertia, $k_m(t)$ corresponds to mesh stiffness, r_b is the base radius, $h[p(t)]$ is the backlash function, and $p(t)$ is teeth deformation along the line of action (LOA). Subscripts 1 and 2 indicate gear 1 and gear 2 property, respectively. Subscripts y, z and x indicate the property direction.

Since the gears' support flexibilities are considered in this paper, teeth deformation is given by:

$$\begin{aligned} p\left(t\right) = {} & (y_1 sen\Psi - y_2 sen\Psi + z_1\cos\Psi - z_2\cos\Psi + r_{b1}\theta_{x1} + r_{b2}\theta_{x2})\cos\left(\beta\right) + \\ & (-x_1 + x_2 + r_{b1}\theta_{y1}sen\Psi + r_{b2}\theta_{y2}sen\Psi + r_{b1}\theta_{z1}\cos\Psi + r_{b2}\theta_{z2}\cos\Psi)\,sen(\beta) - e(t), \end{aligned} \tag{13}$$

where $e(t)$ is the static transmission error, considered here a composition of a mean value, e_m, and a floating value, e_r, which depends on the gear 1 angular position:

$$e(t) = e_m + e_r\sin(\theta_{x1}) \tag{14}$$

Since gear pair may be designed or assembled considering an initial gear tooth distance, called backlash, $2b$, a loss of teeth contact may occur. This condition is described by the backlash function, and is an important source of nonlinear internal excitation of the system Walha *et al.* (2006):

$$h[p(t)] = \begin{cases} p(t) - b, & if\ p(t) > b \\ 0, & if\ -b \leq p(t) \leq b \\ p(t) + b, & if\ p(t) < -b \end{cases} \tag{15}$$

Another internal excitation on geared systems is caused by the mesh stiffness, $k_m(t)$. This stiffness is time-varying due to gear tooth geometry and contact ratio (the number of pairs in mesh).

An analytical method to calculate the spur gear tooth stiffness is the potential energy method. This method considers that the tooth is a variable cross-section beam and the contact force is applied along the contact line at each time instant Yang and Lin (1987). Then, tooth deformation potential energy yields stiffness calculation.

The total potential energy of a tooth subjected to an acting external force is the sum of its bending (b), axial compressive (a) (Yang and Lin, 1987), and shear (s) potential energies (Tian, 2004). Considering the contact of two surfaces, which is the case of a gear pair in mesh, there is also Hertzian energy, h_z (Yang and Lin, 1987). The same idea can be applied to the helical gear tooth, considering it as a series of staggered spur gears (slices), taking into account the helix angle involved, as proposed by Wan *et al.* (2015). Helix angle also causes a variation in the contact line lengths, as shown in Figure 2

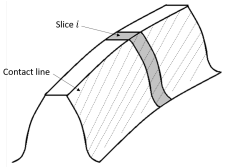

Figure 2. Helical gear tooth

Therefore, the stiffness of a helical tooth (k_{ht}) is:

$$k_{ht} = \left(\sum_{i=1}^{N} \frac{1}{k_{b_i}} \Delta y + \sum_{i=1}^{N} \frac{1}{k_{a_i}} \Delta y + \sum_{i=1}^{N} \frac{1}{k_{s_i}} \Delta y \right)^{-1}, \tag{16}$$

$$\Delta y = l_{ef}/N, \tag{17}$$

where N is the number of spur gear teeth slices that were considered, k_b is the bending stiffness, k_a is the axial compressive stiffness, k_s is the shear stiffness and l_{ef} is the effective contact line length. In this paper, bending, axial, and shear stiffness of the spur gear tooth slice was calculated considering the improved method proposed by Ma *et al.* (2014). Details about contact length calculation are provided by Wan *et al.* (2015).

Tooth pair stiffness is calculated by a series association of pinion and gear stiffness and Hertzian stiffness. Total mesh stiffness, $k_m(t)$ is the sum of the stiffness of pairs in contact at the same time-instant.

3. RESULTS

To simulate the gear pair that generates the high-speed motion for the wind turbine electric generator, a steel helical gear pair is considered (Teng *et al.*, 2014). The helix angle is 15^o, the gears' module is $7mm$ and the face width is $100mm$. Mean (e_m) and floating (e_r) static transmission errors are $10\mu m$ and $0.0001\mu m$, respectively. The driving gear (gear 1) has 54 teeth and an initial speed of $25Hz$, and the driven gear (gear 2) has 21 teeth, also based on Teng *et al.* (2014) data.

The wind turbine drive torque ($T_1(t)$) is considered as a sinusoidal function with a frequency matching the natural frequency of gear 1 torsional vibration mode (ω_n), in order to assess the system's response under critical conditions that could potentially lead to damage:

$$T_1(t) = T_m + T_f(1 + \sin(\omega_n t - \pi/2)), \tag{18}$$

where T_m is the medium torque on gear 1, T_f is the floating torque value and t is the time. In this work, $T_m = 50\ Nm$, $T_f = 2.5\ Nm$ and $\omega_n = 1065\ [rad/s]$. Additionally, an initial load torque of $T_2 = 19.44\ Nm$ (equilibrium condition at $t = 0\ s$) is taken into account to prevent over-speed conditions. Moreover, it is established that this torque would experience a 10% increase if the driven gear rotating speed exceeds 1% of its initial value, which was set to the speed limit.

To solve the system of equations of motion, the Newmark method with middle point rule was used (Walha *et al.*, 2006). Two conditions were simulated: without backlash ($2b = 0$) and with backlash, which was considered to be $2\mu m$. The time step was was initially set at 1×10^{-5} s, but it was decreased by half during the transitions from contact to non-contact conditions and vice versa in the scenario that accounted for backlash. Results are shown and discussed in the following subsections.

3.1 Without backlash

Figure 11 shows the driving torque (a), the load torque (b), the driven gear rotational speed (c), and the line of action (LOA) displacement (d), i.e. $h[p(t)]$, along the time interval considered, which in this case spanned 100 s.

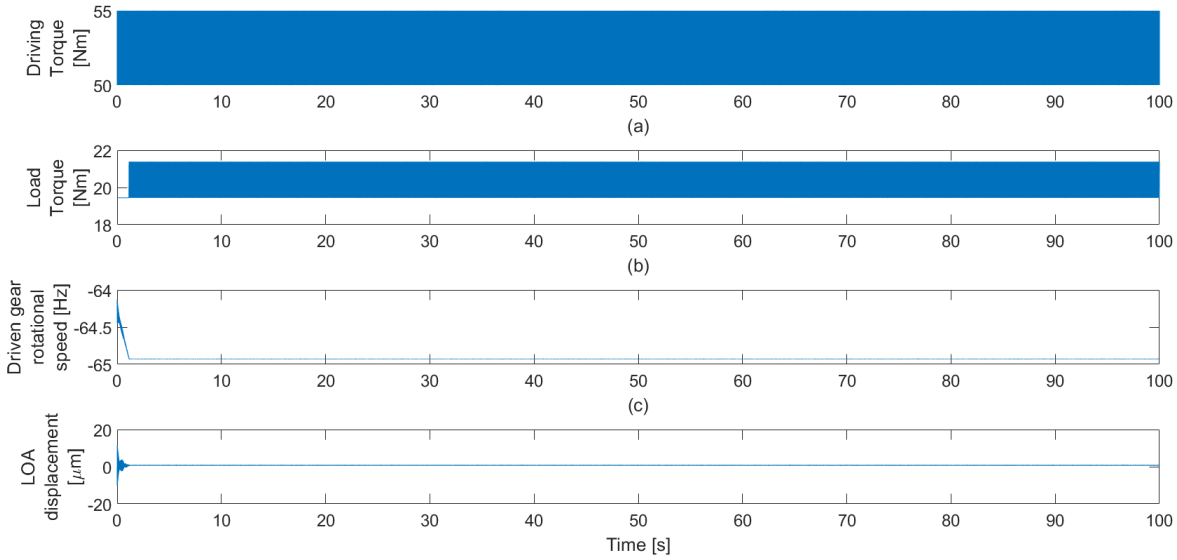

Figure 3. Simulation results of (a) Driving torque; (b) Load torque; (c) Driven gear rotational speed ; (d) LOA displacement for the case considering no backlash

Analyzing the LOA displacement (Figure 3 d), it is possible to notice a transient motion due to the simulation's initial conditions. Result shows that the driven gear rotational speed achieves its maximum at approximately 1 s and then the torque load is increased. After that, the driven gear speed oscillates around this maximum value, and the load torque presents variations to prevent the driven gear speed from exceeding the limit. As the main interest in this paper is the load torque variation effects, the subsequent analysis will focus on the results when the system stabilizes into a steady-state behavior.

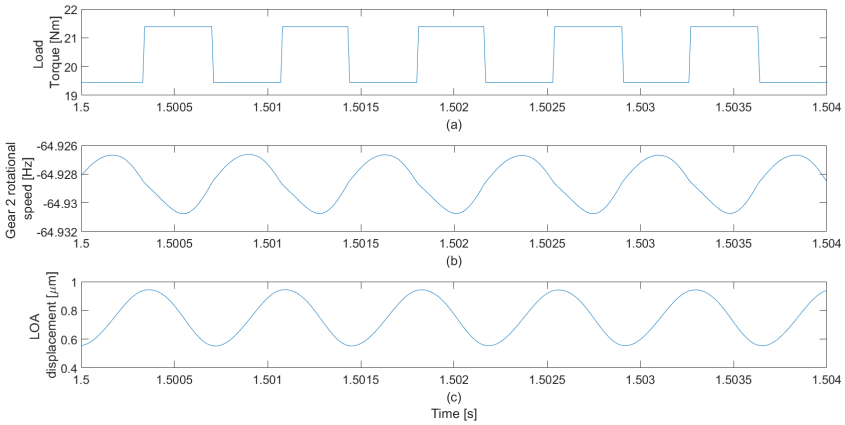

Figure 4. Load torque oscillation (a), Driven gear rotational speed oscillation (b), and LOA displacement oscillation (c) for the case considering no backlash

Figure 4 (a) shows five complete oscillations of the load torque ($T_2(t)$) in a steady-state regime. The same time-

interval is considered to show the driven gear rotational speed (θ_{x2}), as shown in Figure 4 (b), and the LOA displacement ($h[p(t)]$), Figure 4 (c). These figures show that in order to maintain the rotational speed of the driven gear within the specified limit, there are instances where the load torque is temporarily increased. When this occurs, the driven gear rotational speed decreases (in terms of absolute values), and then the load torque returns to its initial value. As a result, the driven gear rotational speed starts to increase again, leading to another increase in the load torque. As a consequence, the LOA displacement also shows an oscillating behavior.

To better understand the dynamical behavior of driving and driven gear, their horizontal (y), vertical (z), and rotation around $x-$axis (θ_x) motions will be analyzed by their phase portrait and Poincaré map. The Poincaré map reference period is the same as the driving torque, $T_1(t)$, period. Axial motion (x_1 and x_2) and rotational motion around y and z axis (θ_{y_1}, θ_{z_1}, θ_{y_2}, and θ_{z_2}) are not analyzed in this paper, since simulation results showed that they can be neglected when compared to the motion in other directions.

Figure 5 displays the phase portrait and the Poincaré map of the driving gear's horizontal motion. The phase portrait shows displacement variations between approximately $-1.08\ \mu m$ and $-0.88\ \mu m$ and speed variations from $-1.3 \times 10^{-4}\ m/s$ to $1.3 \times 10^{-4}\ m/s$. The light blue line shows the phase-portrait of 0.1 s of motion (17 torque cicles). The Poincaré map forms a cloud of points around a closed curve, indicating a quasi-period motion.

A similar result is observed in Figure 6 for the driving gear vertical motion. Displacement variations are between approximately $-11.6\ \mu m$ and $-11.1\ \mu m$ and speed variations from $-3.5 \times 10^{-4}\ m/s$ to $3.5 \times 10^{-4}\ m/s$. The phase portrait of the driving gear rotational motion (Fig. 7) is different from the translational ones: it is possible to see a relation between the angular displacement and the angular speed. The Poincaré map (Fig. 7), presents dots along the entire phase portrait, also indicating a quasi-periodic motion.

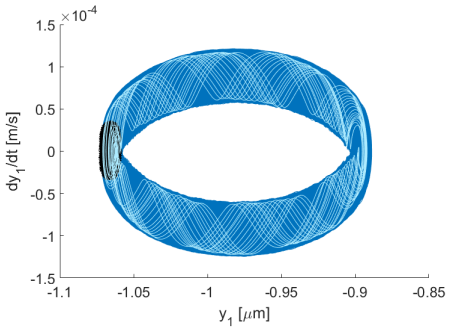

Figure 5. Driving gear horizontal motion for the case considering no backlash. Dark blue: entire time interval phase portrait; Light blue: $0.1\ s$ phase portrait; Black: Poincaré map.

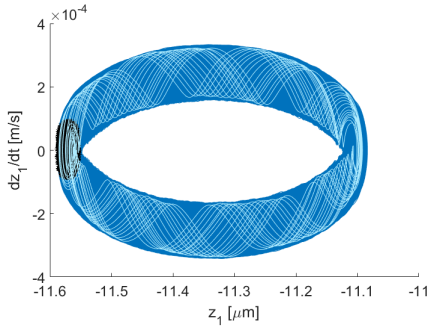

Figure 6. Driving gear vertical motion for the case considering no backlash. Dark blue: entire time interval phase portrait; Light blue: $0.1\ s$ phase portrait; Black: Poincaré map.

Driven gear phase portrait of horizontal (Fig. 8) and vertical motion (Fig. 9) present smaller displacements and velocities amplitudes when compared to the driving gear.

3.2 With backlash

At this point, backlash is taken into consideration. Figure 11 shows the driving torque (a), the load torque (b), the driven gear rotational speed (c), and the line of action (LOA) displacement (d), i.e. $h[p(t)]$, along the time interval considered, which is this case spanned $19.8\ s$.

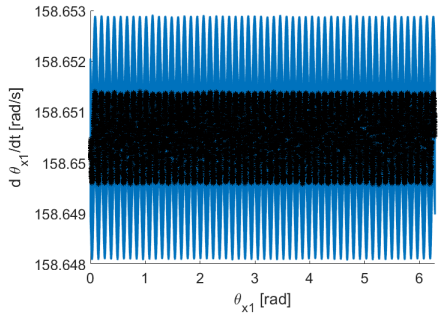

Figure 7. Driving gear rotational motion for the case considering no backlash. Dark blue: entire time interval phase portrait; Black: Poincaré map.

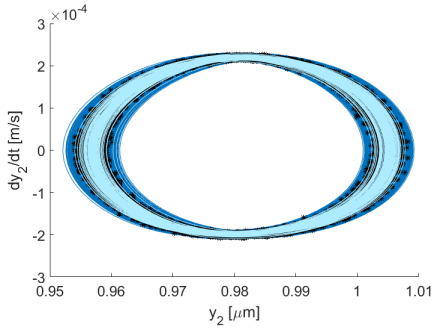

Figure 8. Driven gear horizontal motion for the case considering no backlash. Dark blue: entire time interval phase portrait; Light blue: $0.1\ s$ phase portrait; Black: Poincaré map.

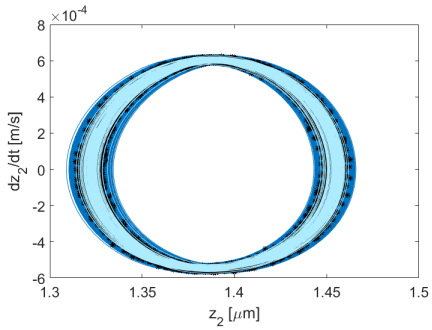

Figure 9. Driven gear vertical motion for the case considering no backlash. Dark blue: entire time interval phase portrait; Light blue: $0.1\ s$ phase portrait; Black: Poincaré map.

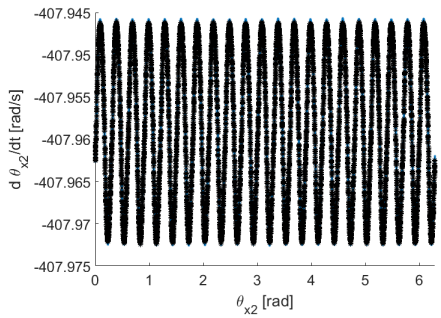

Figure 10. Driven gear rotational motion for the case considering no backlash: (a) Phase portrait. (b) Poincaré map.

LOA displacement, shown in Figure 11 (d), presents a transient motion within the first 0.4s that occurs due to the simulation's initial conditions. The driven gear rotational speed achieves its maximum at approximately 1s and then the

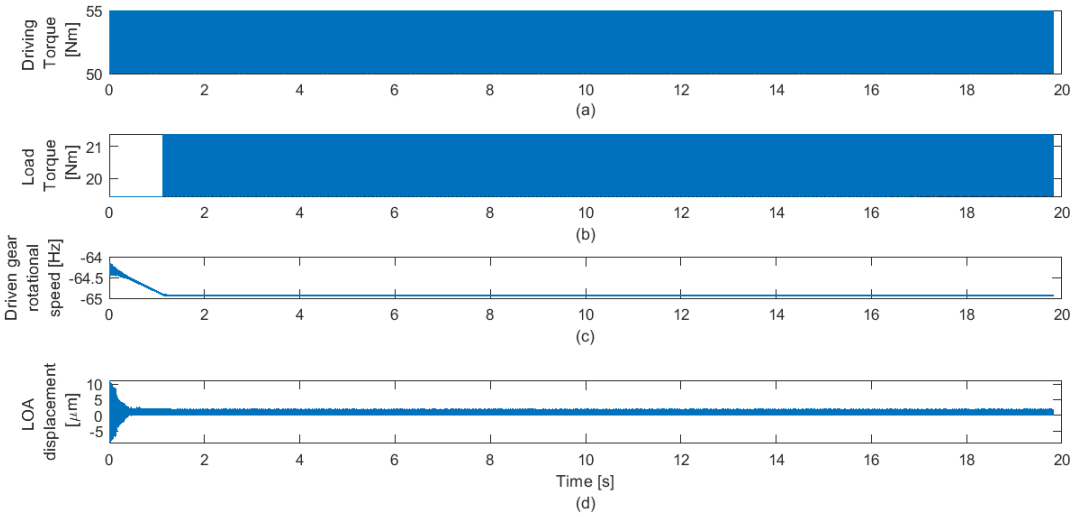

Figure 11. Total time simulation results of (a) Driving torque; (b) Load torque; (c) Driven gear rotational speed ; (d) LOA displacement

torque load is increased. As a consequence of the load torque variation, both the load torque, Figure 11 (b), and driven gear rotational speed, Figure 11 (c), exhibit oscillatory behavior, similar to what is observed in the no backlash condition. The subsequent analysis is focused on the steady state regime.

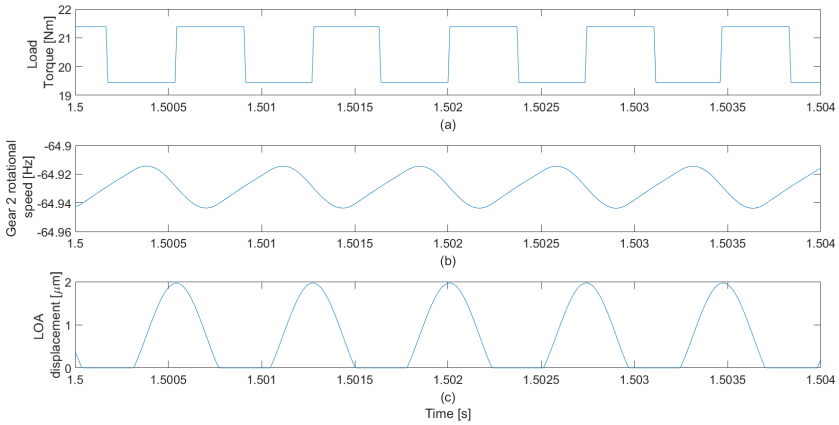

Figure 12. Load torque oscillation (a), Driven gear rotational speed oscillation (b), and LOA displacement oscillation (c)

Figure 12 displays five oscillations of load torque (a), driven gear rotational speed (b) and LOA displacement (c), similarly to Figure 4. In the presence of backlash, the difference is that LOA displacement exhibits not only regions of positive displacement but also periods with no contact ($h[p(t)] = 0$), indicating single-sided impacts on the gear system.

Figure 13 displays the phase portrait (dark blue line), 0.1 s system response phase portrait (light blue line) and the Poincaré map (black dots) of the driving gear's horizontal motion. The phase portrait shows displacements variations between approximately -1.1 μm and -0.88 μm and speed variations from -3×10^{-4} m/s to 3×10^{-4} m/s. The velocity variation is more than twice as pronounced when compared to the case without backlash, and the phase space is entirely filled with trajectories. The Poincaré map corresponds to a circle in a limited region of the phase portrait, indicating quasi-periodic motion. A similar result is shown in Fig. 14, for the driving gear vertical motion, with the phase portrait entirely filled with trajectories (dark blue line) and a circle restrained in a specific region in the Poincaré map. The phase portrait of the driving gear rotational motion and the Poincaré map, Figure 15, are similar to the no-backlash condition, shown in Figure 7.

Driven gear motion in this case is similar to the no-backlash condition. Horizontal and vertical motion phase portrait and Poincaré map (Figures 16 and 17, respectively) exhibit an orbit, indicating quasi-periodic motion. The difference is that there are fewer variations, both in displacement and speed. Rotational motion (Figure 18) also exhibits a restrained trajectory.

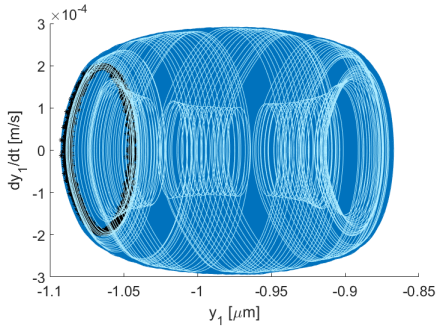

Figure 13. Driving gear horizontal motion for the case considering backlash. Dark blue: entire time interval phase portrait; Light blue: 0.1 s phase portrait; Black: Poincaré map.

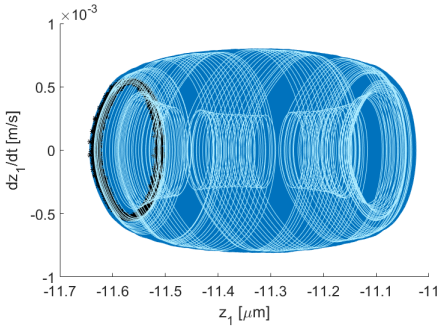

Figure 14. Driving gear vertical motion for the case considering backlash. Dark blue: entire time interval phase portrait; Light blue: 0.1 s phase portrait; Black: Poincaré map.

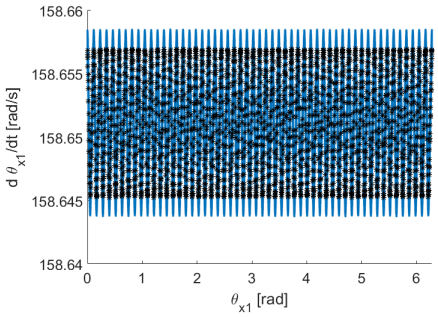

Figure 15. Driving gear rotational motion for the case considering backlash. Dark blue: entire time interval phase portrait; Black: Poincaré map.

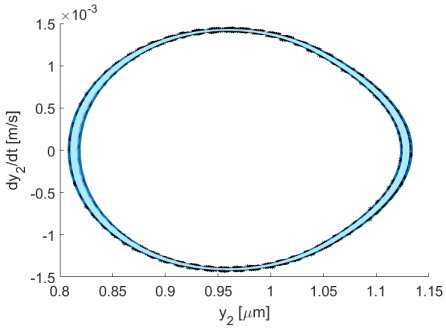

Figure 16. Driven gear horizontal motion for the case considering backlash. Dark blue: entire time interval phase portrait; Light blue: 0.1 s phase portrait; Black: Poincaré map.

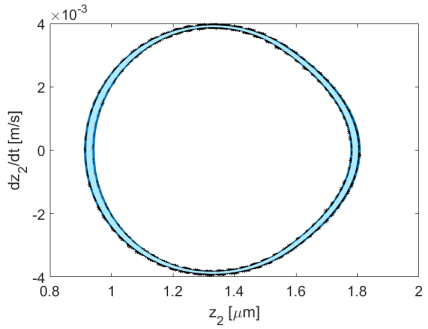

Figure 17. Driven gear vertical motion for the case considering backlash. Dark blue: entire time interval phase portrait; Light blue: $0.1\ s$ phase portrait; Black: Poincaré map.

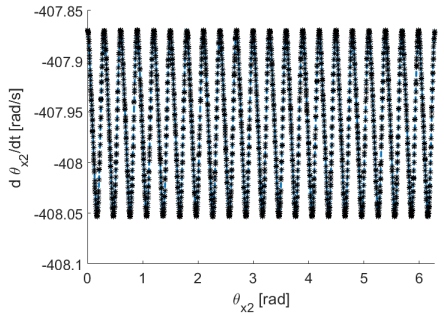

Figure 18. Driven gear rotational motion for the case considering backlash. Dark blue: entire time interval phase portrait; Light blue: $0.1\ s$ phase portrait; Black: Poincaré map.

4. CONCLUSIONS

This paper introduces a lumped parameter model for a helical gear pair, which takes into account a detailed model of the gear mesh, flexibilities in the gear supports, and variable driving and load torques. The primary purpose of this model is to simulate the high-speed stage of a wind turbine gearbox. The gear mesh introduces internal non-linearity into the system, as it accounts for factors such as backlash, time-varying mesh stiffness, and static transmission error. Furthermore, the gear mesh also couples all directions of the gears' motion.

Two conditions were considered: with and without backlash. The presented results showed the time behavior of drive torque, load torque, and LOA displacement. Phase portraits and Poincaré maps of driving and driven gears were analyzed.

In the case without backlash, both driving and driven gears presented indications of quasi-periodic motion. When a backlash is considered, single-sided impacts occurred during the entire period of steady state response, and the driving gear translational motions exhibit a more severe vibration condition with a phase portrait entirely filled with trajectories. To achieve a more comprehensive and quantitative understanding of the system's behavior, it is advisable to employ additional analysis tools beyond the Poincaré map.

These preliminary results show that load torque variations, that may occur on wind turbines to avoid over-speed conditions, may cause damaging effects on the helical gear pair due to non-periodic motion. In the presence of a backlash, impacts and chaotic behavior may occur.

5. ACKNOWLEDGEMENTS

The authors are grateful to the Brazilian National Council of Research (CNPq - Brazil), process 407978/2022-4, to CAPES and FAPDF, process 00193-00001139/2021-57, for their support.

6. REFERENCES

Apata, O. and Oyedokun, D., 2020. "An overview of control techniques for wind turbine systems". *Scientific African*, Vol. 10, p. e00566. ISSN 2468-2276. doi:https://doi.org/10.1016/j.sciaf.2020.e00566.

Kahraman, A., 1994. "Dynamic analysis of a multi-mesh helical gear train". *Journal of Mechanical Design, Transactions of the ASME*, Vol. 116, No. 3, pp. 706–712. ISSN 10500472. doi:10.1115/1.2919440.

Kubur, M., Kahraman, A., Zini, D.M. and Kienzle, K., 2004. "Dynamic analysis of a multi-shaft helical gear transmission

by finite elements: Model and experiment". *Journal of Vibration and Acoustics, Transactions of the ASME*, Vol. 126, No. 3, pp. 398–406. ISSN 10489002. doi:10.1115/1.1760561.

Ma, H., Song, R., Pang, X. and Wen, B., 2014. "Time-varying mesh stiffness calculation of cracked spur gears". *Engineering Failure Analysis*, Vol. 44, pp. 179–194. doi:10.1016/j.engfailanal.2014.05.018. URL http://dx.doi.org/10.1016/j.engfailanal.2014.05.018.

Özgüven, H.N., 1991. "A non-linear mathematical model for dynamic analysis of spur gears including shaft and bearing dynamics". *Journal of Sound and Vibration*, Vol. 145, No. 2, pp. 239–260. ISSN 10958568. doi:10.1016/0022-460X(91)90590-G.

Ragheb, A. and Ragheb, M., 2010. "Wind turbine gearbox technologies". In *2010 1st International Nuclear Renewable Energy Conference (INREC)*. pp. 1–8. doi:10.1109/INREC.2010.5462549.

Teng, W., Wang, F., Zhang, K., Liu, Y. and Ding, X., 2014. "Pitting fault detection of a wind turbine gearbox using empirical mode decomposition". *Strojniški vestnik - Journal of Mechanical Engineering*, Vol. 60, No. 1, pp. 12–20. ISSN 0039-2480. doi:10.5545/sv-jme.2013.1295.

Tian, X., 2004. *Dynamic Simulation for System Response of Gearbox Including Localized Gear Faults*. University of Alberta. URL https://books.google.com.br/books?id=X7PzSgAACAAJ.

Walha, L., Fakhfakh, T. and Haddar, M., 2006. "Backlash effect on dynamic analysis of a two-stage spur gear system". *Journal of Failure Analysis and Prevention*, Vol. 6, No. 3, pp. 60–68. ISSN 15477029. doi: 10.1361/154770206X107325.

Wan, Z., Cao, H., Zi, Y., He, W. and Chen, Y., 2015. "Mesh stiffness calculation using an accumulated integral potential energy method and dynamic analysis of helical gears". *Mechanism and Machine Theory*, Vol. 92, pp. 447–463. ISSN 0094114X. doi:10.1016/j.mechmachtheory.2015.06.011. URL http://dx.doi.org/10.1016/j.mechmachtheory.2015.06.011.

Wang, L., Zuo, S., Song, Y.D. and Zhou, Z., 2014. "Variable torque control of offshore wind turbine on spar floating platform using advanced rbf neural network". *Abstract and Applied Analysis*, Vol. 2014. ISSN 1085-3375. doi: https://doi.org/10.1155/2014/903493.

Wei, S., Zhao, J., Han, Q. and Chu, F., 2015. "Dynamic response analysis on torsional vibrations of wind turbine geared transmission system with uncertainty". *Renewable Energy*, Vol. 78, pp. 60–67. ISSN 18790682. doi: 10.1016/j.renene.2014.12.062. URL http://dx.doi.org/10.1016/j.renene.2014.12.062.

Yang, D.C. and Lin, J.Y., 1987. "Hertzian damping, tooth friction and bending elasticity in gear impact dynamics". *Journal of Mechanical Design, Transactions of the ASME*, Vol. 109, No. 2, pp. 189–196. ISSN 10500472. doi: 10.1115/1.3267437.

Zhao, M. and Ji, J., 2015. "Nonlinear torsional vibrations of a wind turbine gearbox". *Applied Mathematical Modelling*, Vol. 39, No. 16, pp. 4928–4950. ISSN 0307-904X. doi:https://doi.org/10.1016/j.apm.2015.03.026.

7. RESPONSIBILITY NOTICE

The authors are solely responsible for the printed material included in this paper.